Design, Construction and Test of a Magnetically Geared Induction Machine

Badr-El-Boudour Bidouche, Thierry Lubin, Franck Vangraefschepe, Smail Mezani, Tahar Hamiti

Design, Construction and Test of a Magnetically Geared Induction Machine

Badr-El-Boudour Bidouche
Université de Lorraine - GREEN
F-54000 Nancy, FRANCE
badr.bidouche@univ-lorraine.fr

Thierry Lubin
Université de Lorraine - GREEN
F-54000 Nancy, FRANCE
thierry.lubin@univ-lorraine.fr

Smail Mezani
Université de Lorraine - GREEN
F-54000 Nancy, FRANCE
smail.mezani@univ-lorraine.fr

Franck Vangraefschepe
previously VEDECOM employee
IRT Saint-Exupery
Toulouse, FRANCE
franck.vangraef@irt-saintexupery.com

Tahar Hamiti
Nidec PSA emotors
Carrières-sous-Poissy, FRANCE
tahar.hamiti@emotors.com

***Abstract*—This paper describes the realization and the test of a 1 kW- 45 rpm magnetically geared induction machine. The principle of operation and the design procedure are firstly described, then the prototype construction is detailed. Finally, measurement results are presented and compared to the computations under full load conditions. It is the first prototype for this type of machine never built and tested under rated condition.**

Keywords— magnetic gear, induction motor, design, prototype, experimental results.

I. Introduction

High performance magnetic gears combined to electrical machines have been proposed to replace the usual system which consists of an electrical machine and a mechanical gear. The association of a synchronous machine (PM machines are mostly used) to a magnetic gear leads to a high torque density system for several applications [1]-[5].

There are numbers of industrial applications where it is well suited to employ an induction motor which present the advantage of self-starting when connected to the network. Hence, a new concept called magnetically geared induction machine (MaGIM) was first introduced in [6] and [7]. It combines an induction machine with a magnetic gear to achieve a high-torque/low-speed drive.

The electromagnetic and thermal design of the MaGIM rated at 1 kW - 45 rpm was described in [8] by means of analytical and finite element computation tools. This MaGIM is intended for a constant speed operation on the 400 V-50 Hz network. A simplified lumped-parameter thermal model was built to estimate the temperature of the machine.

The dynamic behavior of the MaGIM was presented in [9] using an analytical model. This model is used to predict the transient performance for a direct-on-line starting and for a sudden change of load torque. A stability analysis of the system was also carried out.

In this paper, we present the construction of a prototype to validate the design procedure of the MaGIM. To the best knowledge of the authors, it is the first prototype for this type of machine never built and test under full load condition. In a first section, we recall the working principle of the MaGIM. Then we present a summary of the design procedure. In a third section, we present the construction of the MaGIM, and we finally give experimental results for the machine connected to the grid under full load condition.

II. Working Principe of MaGIM

The structure of the MaGIM is shown in Fig. 1. It consists of a wound-rotor induction motor (IM) with inverse topology (internal stator and external rotor) and an integrated magnetic gear. The motor constitutes the internal part, whereas the magnetic gear represents the outer part of the MaGIM. The high-speed rotor is the common part of the induction motor and the magnetic gear.

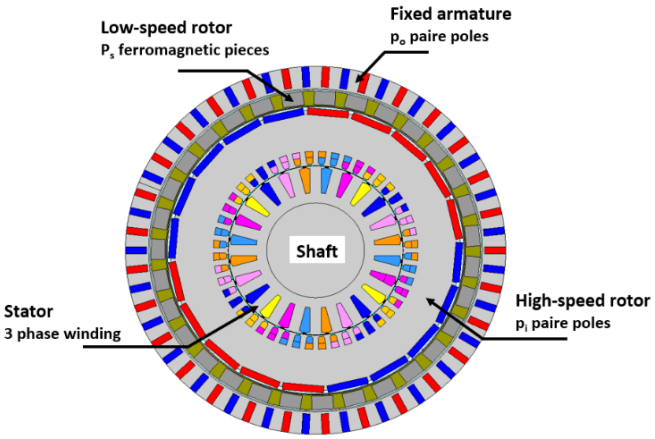

Fig. 1. 2D cross section view of MaGIM

The MaGIM is composed of four armatures; two of them being stationary and the two others are rotating:

- The inner armature represents the stator of the induction machine whose 3-phase winding is connected to the grid (8-pole machine).
- The rotor of the IM rotates at high speed (HS). On the external surface of this HS rotor, p_i pole-pairs permanent magnets are mounted.
- The low speed (LS) rotor consists of P_s ferromagnetic pole-pieces embedded in a fiberglass container.
- The external armature is fixed. It consists of p_o pole-pairs permanent magnets disposed in a flux focusing configuration to facilitate the assembly of the device and to reduce its dimensions. In fact, the flux density in the air gap can be significantly increased using a flux focusing outer rotor, allowing to reduce the size of the magnetic gear.

A flux-focusing magnetic gear using ferrite magnets with a gear ratio of 4.25 has been studied in [10]. An analysis of the variations of the torque and its density for different shaft diameters and different types of magnets was presented. Then, a prototype was constructed in [11] where a torque density of 239 Nm/L was obtained by optimizing the coaxial magnetic gear presented in [10], with a relatively small air gap (0.5 mm), and NdFeB type magnets of 1.25T.

The principle of operation of the magnetic gear is based on the modulation of the magnetic field created by the p_i PM pole-pairs by the Ps ferromagnetic pole-pieces. The obtained field interacts with the p_o PM pole-pairs of the external armature to transmit torque to the low-speed load [1].

The wound rotor induction motor has a p pole-pairs three-phase windings in the stator and the rotor armatures. The electromagnetic torque produced by in the IM moves the high-speed rotor at a mechanical speed ω_i. The external armature being held stationary, the torque is transmitted to the low-speed load via the pole-pieces. This torque corresponds to the one imposed by the load at a speed ω_s. It is important to note that the net average torque on the high-speed rotor (motor + magnetic gear) is equal to zero if viscous friction losses are neglected. The speeds ω_i and ω_s are related by [1]:

$$\omega_i = \frac{P_s}{P_s - p_o}\,\omega_s \tag{1}$$

Thus, the resulting gear ratio G_r is:

$$G_r = \frac{P_s}{p_i} \tag{2}$$

III. Design Procedure of the MaGIM

Given the complexity of the MaGIM, the two sub-systems (the IM and the magnetic gear) were considered magnetically decoupled [8]. Therefore, they were designed separately.

The geometrical parameters of the induction machine were determined using the classical formulas for the design of electrical machines [12]. The magnetic gear was sized using an analytical model based on the sub-domain method [13].

A parametric optimization was performed to determine the thicknesses of the magnets and the ferromagnetic pole-pieces along with their opening angle [8]. The maximum transmissible torque was also determined to set the final gear dimensions. Given the importance of 3D effects, a 3D finite element analysis (FEA) was carried out using a magnetic scalar potential formulation.

Analytical 2D and 3D FEA calculations give a static sinusoidal torque with practically no ripple. The 2D analytical model gives a maximum torque of 350 Nm while the 3D FEA gives 310 Nm which corresponds to 13% relative difference (the reference value is the torque calculated in 3D). After all, the 30% margin considered in the 2D calculation to account for the 3D effects has been greatly overestimated. Finally, we kept these dimensions, which allows us to increase the stability margin of the magnetic gear [8]. In fact, the 30% overload capacity initially foreseen during the design process by 2D calculation increases to 40%.

During this sizing procedure, a compromise was done between the performances of the IM and the magnetic gear in order to have acceptable energetic performances of the MaGIM [8]. An FE analysis of the overall system was performed in order to get more precise results. At rated operation, the MaGIM delivers 210 Nm and 45 rpm on the low-speed rotor. The slip of the IM is about 8%, which corresponds to a speed of 690 rpm of the high-speed rotor.

A non-linear-time-stepping 2D FE simulation with movement consideration and circuit coupling was also performed for the whole system. Figure 2(a) shows the dynamic torque waveform of the low speed rotor. This torque is practically ripple free with a mean value of 210 Nm, the torque ripples don't exceed 1%. Figure 2(b) presents the total torque exerted on the high-speed rotor. Of course, the mean torque is equal to zero since the gear and the machine develop opposite torques whose mean values are about 14 Nm. However, one can observe in Fig. 2(b) torque ripples of around 4 Nm due to the machine and gear sides. These ripples represent 26% of the rated torque of 14 Nm. This point highlights one of the great peculiarities of magnetic gears. The magnetic gear can transmit ripple-free torque to the load via the low-speed rotor, while the input torque on the high-speed rotor exhibits significant pulsation values.

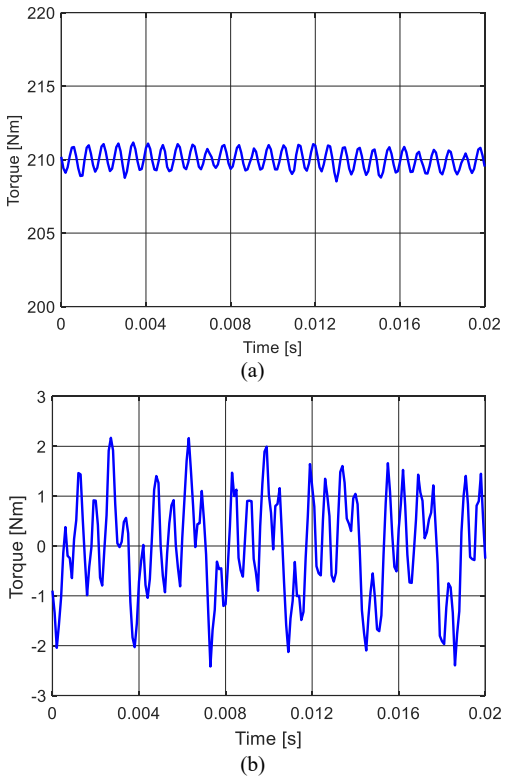

Fig. 2. Non-linear-time-stepping 2D FE simulations of the whole system (a) Low-speed rotor dynamic torque ; (b) High-speed rotor dynamic torque.

The analytical transient model of the MaGIM, which contains the mechanical equations of the IM and magnetic gear was presented in [9]. The dynamic steady-state model of the IM was established in Park's reference frame. As for the non-linear analytical model of the magnetic gear, it is based on the laws of mechanics of rotating systems and is written as a function of the load angle. We have seen that the MaGIM can start on the grid under full voltage and that this start depends strongly on the moment of inertia of the load J_l. The expression of the critical pulsation was determined by linearizing the dynamic model of the magnetic gear. Finally, the behavior of the device was studied when a load step torque is applied. This study allows to highlight the stall phenomenon of the MaGIM and the peculiarity of magnetic gears to protect themselves against overloads [9].

The MaGIM parameters obtained along with the design procedure were presented in [8]. The main geometrical parameters are given in Table 1. We showed that the right choice of the combination (p_o, p_i, P_s) allowed us to reach the desired torque value with reduced ripples. Because of the high rotor temperature [8], Samarium-Cobalt magnets have been selected for the inner rotor. This system has a torque density of about 26 Nm/L, which is almost twice the density of a classical system combining an IM with a mechanical gear. Indeed, a mechanical gear with the same gear ratio exhibits a torque density of about 15 Nm/L [13]. When associated to a high-speed induction motor having a standard torque density of 10 Nm/L, the overall system (IM + mechanical gear) will exhibit a torque density of 14 Nm/L. This clearly shows that MaGIM is superior to the conventional system combining an IM with a mechanical gear with a torque density almost twice, with the benefit of better reliability and low maintenance requirements.

TABLE 1
MAIN GEOMETRICAL PARAMETERS OF THE CONSTRUCTED MAGIM

Magnetic gear side	
Inner rotor pole-pairs p_i	2
Stationary armature poles-pairs p_o	29
Number of pole-pieces P_s	31
Gear ratio G_r	15.5
Inner Airgap	2 mm
Outer Airgap	1.5 mm
Remanence inner rotor PMs (SmCo)	1.1 T
Remanence external armature PMs (NdFeB)	1.3 T
External radius	135 mm
Inner rotor radius	80.5 mm
Active length	150 mm
Induction machine side	
Stator rated line voltage (Y connexion)	400 V
Suply frequency	50 Hz
Pole pairs p	4
Active length	150 mm
Stator outer radius	62.3 mm
Airgap	0.35 mm
Number of stator slots	24
Number of rotor slots	48
Stator turns per phase	296
Rotor turns per phase	160

IV. REALIZATION OF THE MAGIM PROTOTYPE

The goal of this paper is to validate the design by building a small prototype. This prototype of 1kW will operate on the 400V - 50 Hz network. It should deliver a torque in excess of 210 Nm at a rotation speed of about 45 rpm. The construction of such a structure which has three airgaps is challenging.

Fig.3 shows the axial half-section view of the prototype. It is composed of an active part having the four armatures described above.

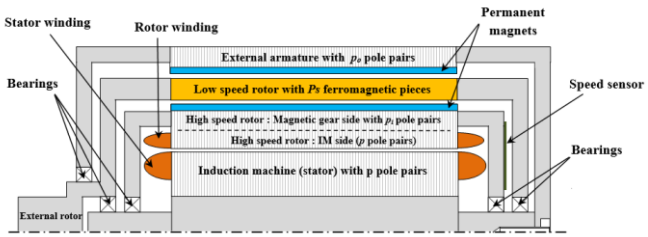

Fig. 3. Structure of the MaGIM's prototype

A. Active part construction

The active parts of the MaGIM are supported by a central shaft through ball-bearings. This shaft has a hollow side as to thread different leads connected to stator phases, speed sensor and thermocouples. The shaft is made of stainless steel to reduce magnetic interactions with the stator and HS rotor end-windings.

The stator is mounted on the shaft and blocked with a metallic rod (Fig.4). The three-phase stator winding (single-layer, full-pitch) is distributed in 24 slots which are skewed by 7.5° (one rotor tooth pitch) to reduce the torque pulsations of the IM. The stator iron consists of M400 50A FeSi laminations. It is separated from the high-speed rotor by an air gap of 0.35 mm.

The HS rotor (Fig 5) has 48 straight slots in which the short-circuited three-phase winding (double-layer, 5/6 shortened pitch) is distributed. It is also made from M400 50A FeSi laminations. The permanent magnets are mounted on the HS rotor surface. SmCo S300 rectangular magnets with constant magnetization are used. Each pole consists of 15 rectangular segments (5 in the ortho-radial direction and 3 in the axial direction) in order to limit the eddy current losses.

The low-speed rotor (Fig. 6) consists of a slotted fiberglass container (G11) in which ferromagnetic pole-pieces manufactured from Soft Magnetic Composite material are inserted and glued. These pieces are axially segmented into two parts to simplify assembly and prevent breakdown.

The last part concerns the external armature (Fig. 7). The laminations are slotted, the straight slots have an internal bridge of 0.5 mm. Rectangular N42-NdFeB permanent magnets, magnetized in the ortho-radial direction are inserted in the slots. As we can see in Fig.8, these laminations are attached to external fixations on the left and on the right side by means of solid crowns of the same diameter and 20 mm thickness. The right external fixation fasten the armature to the shaft with 8 screws, while the left-one allows the external armature to rest on the output shaft through a bearing. This configuration is chosen to simplify the construction. Indeed, the magnets are inserted and glued in the slots once the MaGIM is completely assembled (Fig.9).

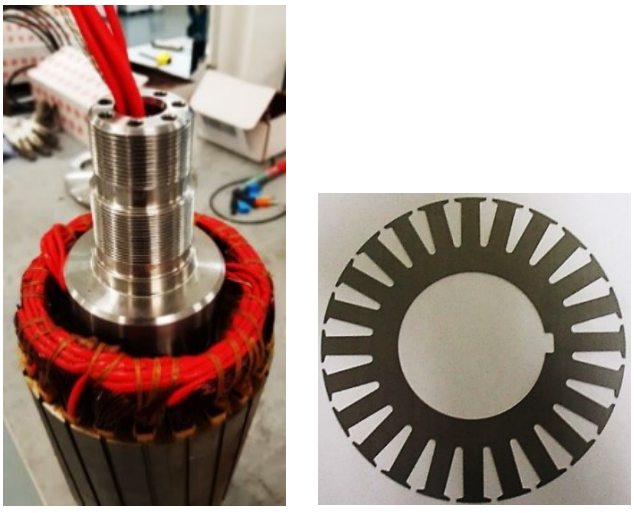

Fig. 4. Inner stator mounted on the shaft with coils connections

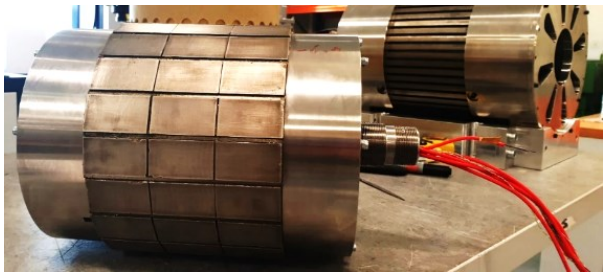

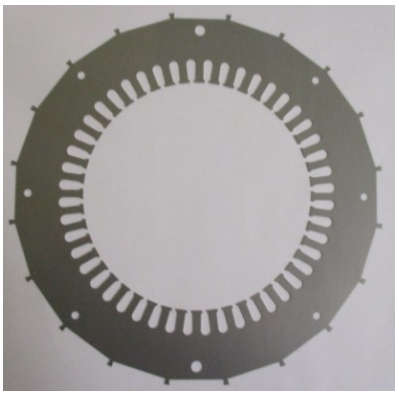

Fig. 5. High-Speed rotor and its ferromagnetic lamination

Fig. 6. Low speed rotor in G11 with ferromagnetic pole-pieces.

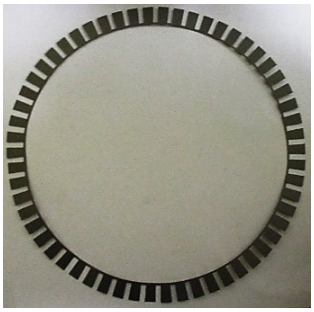

Fig. 7. Stationary external armature and its ferromagnetic lamination.

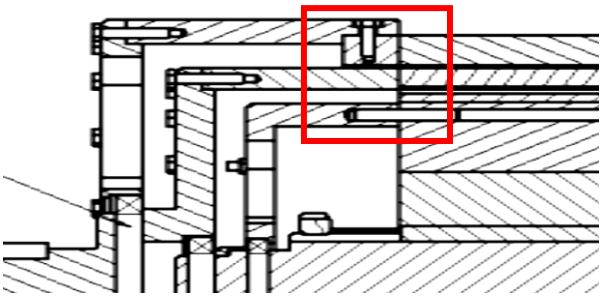

Fig. 8. Fixation of the external armature.

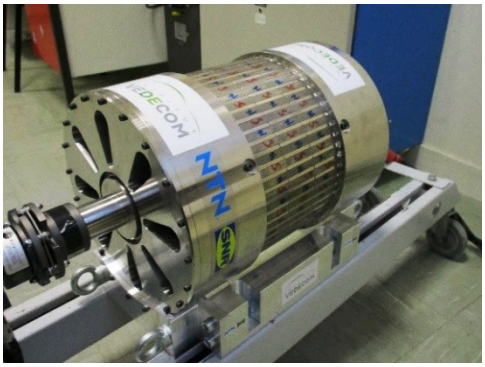

Fig. 9. MaGIM prototype (1 kW, 45 rpm, 210 Nm).

B. Measurement apparatus and sensors

The high-speed rotor is not accessible to simplify the construction. Hence, in order to get the speed and position of this rotor, we integrated a MPS40S speed sensor manufactured by NTN-SNR (Fig. 10). This sensor consists of two parts:

- the first is the 96-pole rotating magnet ring mounted on the HS rotor (black ring in Fig. 10)

- the second part consists of a Hall sensor attached to a stationary PCB Board which measures the field variation due to ring magnet rotation. This allows the determination of the position variation from which the speed is deduced. An electronic chip glued on the PCB ensures signal processing. This sensor has a resolution of 0.1875 degrees.

Stator temperature measurements are also carried out using five K-type thermocouples located in the slots and end-windings. The thermocouple leads are connected to a signal conditioning interface called "Graphtech" which allows the recording of the measured temperatures (Fig. 21).

The low-speed torque is measured using a torque sensor of type DR-2112 from SCAIME (Fig. 11). One side is connected to the output shaft of the MaGIM and the other side is connected to the load via a flexible coupling. This torque-meter can measure torque values up to 500 Nm in both steady state and transient conditions.

V. Experimental Results

The MaGIM prototype is placed in a test bench shown in Fig.11. A DC machine rated 3kW-1500 rpm is used as a mechanical load (generator mode) or as a driving motor. To adapt the low speed output torque of the MaGIM to the DC machine high-speed, a mechanical gear having a gear ratio of 15.8:1 and a rated torque of 500 Nm is employed. The torque-meter is placed between the MaGIM and the low-speed side of the mechanical gear.

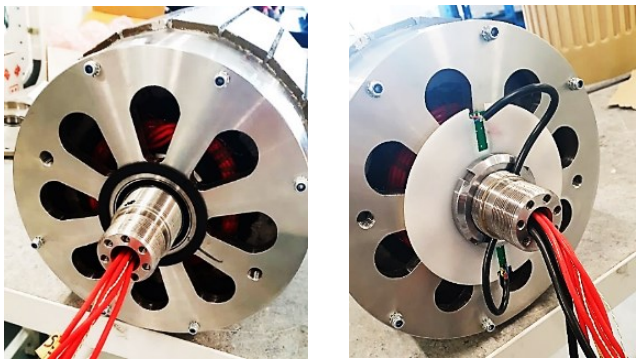

Fig. 10. HS rotor speed sensor (magnet sensor).

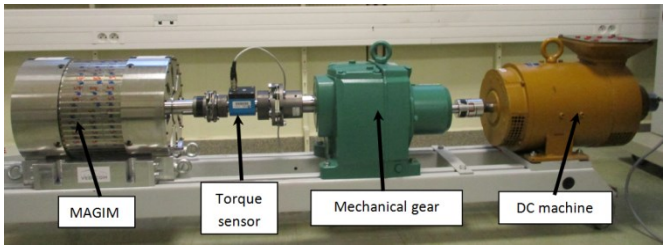

Fig. 11. Test bench of the MaGIM.

A. Static torque measurement

The purpose of this test is to measure the MaGIM's low-speed rotor torque at different rotor positions. In order to carry out this test, the high-speed rotor is locked by a stainless-steel rod. We apply a torque on the low speed rotor by controlling the armature current in the dc machine as shown in Fig.12. A DSP board (DS1104 from DSpace) is used to ensure the current and torque control of the dc machine which is supplied via a Buck dc converter.

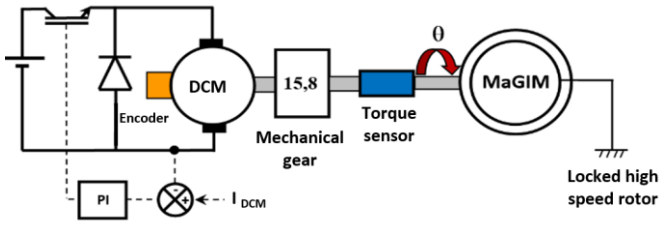

Fig. 12. Static torque measurement.

In so doing, the low-speed rotor moves from its initial position to a stable final position which corresponds to the applied torque (under stable operation). In practice and starting from a zero torque, small current steps are applied to the dc machine. The torque and position variations vs. time are then recorded. Fig. 13 and Fig. 14 show the torque and position response respectively. It can be noted that a stable state is reached after around 0.1 s. This is due to the dynamic properties of the experimental bench (moments of inertia and friction). It can be noted that the system is very damped (no oscillations of the position response), certainly due to the high friction coefficient of the mechanical gear.

Fig. 15. shows the computed (2D FE) and measured steady state torque vs. position curves of the low speed rotor (static torque). The agreement is good as the relative difference does not exceed 5% in the worst case. The measured maximum value is about 330 Nm while the computed one is 310 Nm

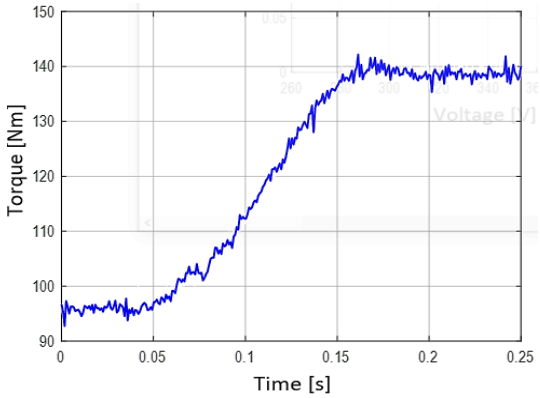

Fig. 13. MaGIM's low-speed rotor torque variation

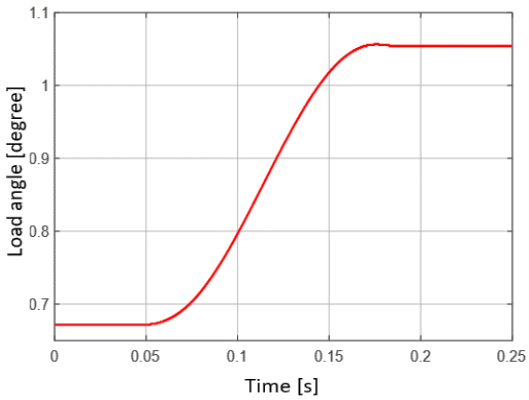

Fig. 14. MaGIM's low-speed rotor position variation

B. Locked-rotor and No-load tests

The classical no-load and locked-rotor tests were performed to determine the electrical parameters of the MaGIM equivalent circuit as shown in Fig. 16 (where g is the slip). The no-load test has been done for different values of the stator voltage (50Hz) and with the MaGIM alone (without mechanical load) to have a good determination for the iron and mechanical losses that can be separated from this test.

The experimental results are given in Table 2 (R_f was not determinate by the analytical model). The mechanical losses of the MaGIM are around 150W at rated speed whereas the iron losses are equal to 45W for the rated voltage (400V/50Hz). One can observe in Table 2 that the electrical parameters obtained by measurement are in good agreement with the ones obtained analytically [8].

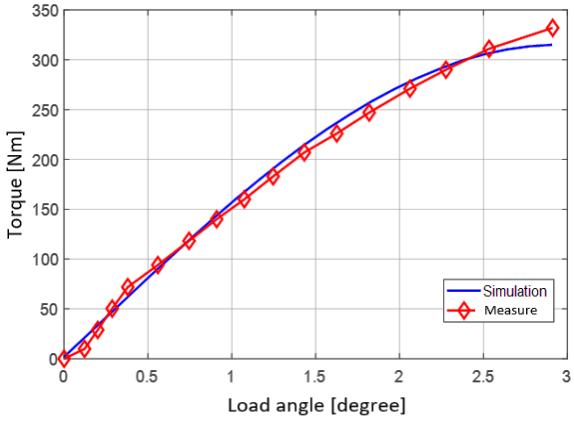

Fig. 15. Static torque measurement of the low-speed rotor

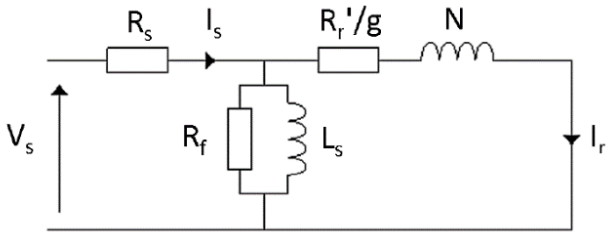

Fig. 16. Per-phase equivalent circuit of the MaGIM

TABLE 2
ELECTRICAL PARAMETERS OF THE MAGIM

	Rs (Ω)	Rf (kΩ)	Ls (mH)	Rr' (Ω)	N (mH)
Measurement	4.5	3.7	0.22	5.8	42
Analytical	4.9	-	0.24	6.4	47

C. *Full-load test*

This test is made with the MaGIM connected to the grid (400V/50Hz). The DC generator shown in Fig. 11 acts as a load. The stator power is measured with a PA4000 Power analyzer as shown in Fig. 18. Speed and load torque measurement are obtained as explained in the previous part.

Fig. 17 compares the torque versus the rotor speed obtained by measurement and by the analytical model (equivalent circuit of Fig. 16). One can observed that the full load (210 Nm, 44 rpm) has been reached with the proposed prototype. Moreover, we can see that the measurement agrees very well with the prediction. The slip speed at full load is around 10% as expected in [8]. Power measurement for the three phases obtained with the PA4000 (Fig. 18) shows that the stator circuit is well balanced, we can note the same stator currents values and the same powers for the three phases. Results given in Fig. 18 correspond to the full load condition. The total input power is equal to 1750W and the mechanical power is equal to 968W (210Nm@44rpm), that corresponds to an efficiency of around 55%, which is not very far of our target during the design process (60%) [8]. It is important to note that the efficiency of a standard induction machine with a power around 1kW and 4 pole-pairs is around 70%, without considering the mechanical gear efficiency. Fig. 19 and Fig. 20 respectively give the RMS current and the power factor of the MaGIM versus slip. Once again, measurements and predictions are in good agreement. The power factor reaches a value of 0.6 at full load, which is not far from the one obtained with a classical 8-poles induction machine with the same power (around 0.65). Finally, Fig. 21 shows that the winding temperature in the slot at full load is not greater than 74°C and the temperature for the end-winding is around 65°C under steady state condition.

VI. CONCLUSION

In this Paper, the construction and test of a 1kW-45 rpm MaGIM prototype has been presented. The purpose of this experimental work is to validate the concept of the MaGIM, and the methodology used for its design. The realization of this complex device required more than a year of work which included technical choices and drawings, active parts and casing assembly, set up of the measurement apparatus and tests.

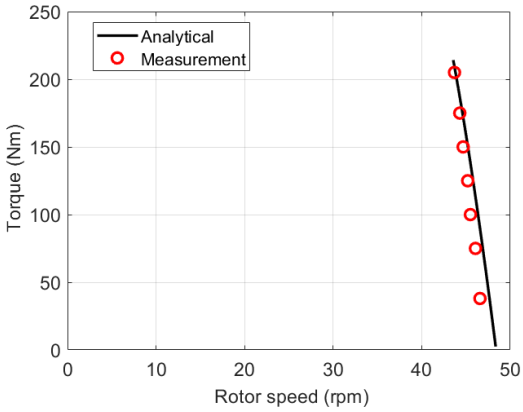

Fig. 17. Load torque versus rotor speed.

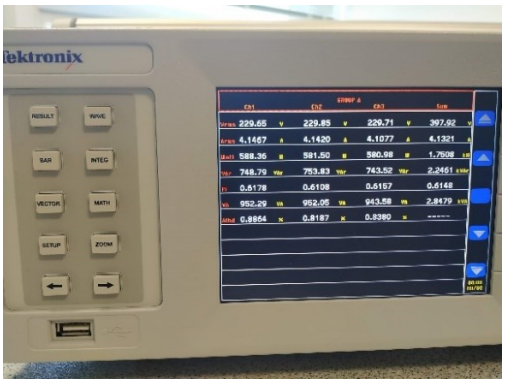

Fig. 18. Input power measurement for full load condition (PA4000).

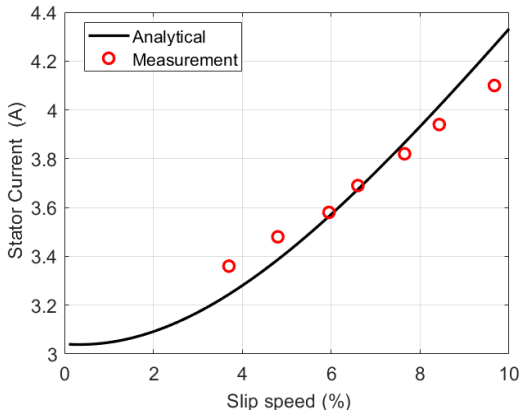

Fig. 19. Stator current versus slip speed.

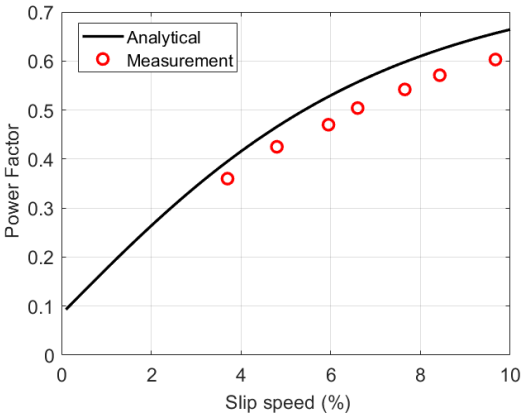

Fig. 20. Power factor versus slip speed.

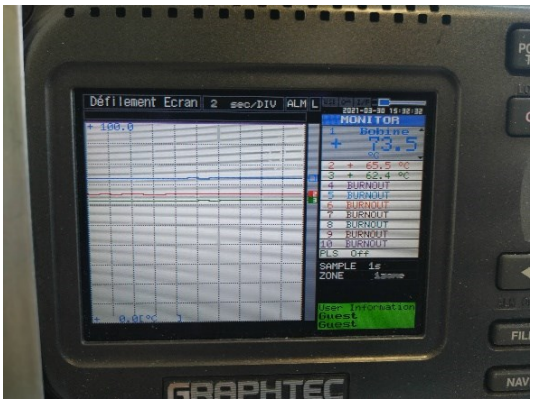

Fig. 21. Coils temperature measurement for full load condition.

Results obtained for the static torque measurement and under full load condition when the machine is connected to the grid are very satisfactory. Indeed, the measured and calculated results are in very good agreement. For full load condition, we obtained an efficiency of 55% and a power factor equal to 0.6, which are not very far compared to a standard induction machine of the same category (1kW, 8-poles) including the mechanical gear. Moreover, this system has a torque density of 26 Nm/L, which is almost twice the density of a classical system combining an IM with a mechanical gear. The efficiency versus complexity and cost of this type of machine will have to be compared in the future with other original machines currently under study [14].

ACKNOWLEDGMENT

The authors gratefully acknowledge the contributions of VEDECOM Mobilab for the realization of the prototype, NTN-SNR for the HS rotor speed sensor, and Polytech'Nancy for the technical drawings.

REFERENCES

[1] K. Atallah and D. Howe, "A Novel High-Performance Magnetic Gear," *IEEE Trans. Magn*., Vol. 37, No. 4, pp. 2844–2846, Jul. 2001.

[2] P. O. Rasmussen, T. O. Andersen, F. T. Jorgensen, and O. Nielsen, "Development of a high-performance magnetic gear," *IEEE Trans. Ind. Appl*., vol. 41, no. 3, pp. 764–770, May/Jun. 2005.

[3] K. Atallah, J. Rens, S. Mezani, D. Howe, "A Novel 'pseudo' direct-drive brushless permanent magnet machine," *IEEE Trans. Magn.*, vol. 44, no. 11, pp. 4349-4352, Nov. 2008.

[4] Z. Q. Zhu, "Overview of novel magnetically geared machines with partitioned stators," *IET Electr. Power Appl.,* Vo. 12, No 5, pp. 595 – 604, 2018.

[5] M. Johnson, M. C. Gardner, H. A. Toliyat, S. Englebretson, W. Ouyang, C. Tschida, " Design, Construction, and Analysis of a Large-Scale Inner Stator Radial Flux Magnetically Geared Generator for Wave Energy Conversion," *IEEE Trans. on Ind. Appl*., Vol. 54, No 4, pp. 3305-3314, 2018.

[6] S. Mezani, T. Hamiti, L. Belguerras, T. Lubin, M. Rashed and C. Gerada,"Magnetically Geared Induction Machines," *IEEE Trans. Magn*, vol. 51, no. 11, 8111404, Nov. 2015.

[7] D. Z. Abdelhamid, and A. M Knight, "Performance of a High Torque Density Induction Motor with an Integrated Magnetic Gear". *2016 XXII International Conference on Electrical Machines (ICEM)*, Lausanne, Switzerland, 4–7 September 2016; pp. 538–544

[8] B. Bidouche, T. Lubin, S. Mezani, "Design and Analysis of a Magnetically Geared Induction Machine", *2018 XIII International Conference on Electrical Machines (ICEM)*, Alexandroupoli, Greece.

[9] B. Bidouche, T. Lubin, S. Mezani, "Dynamic behaviour of a Magnetically Geared Induction Machine". 19th *International Symposium on Electromagnetic Fields in Mechatronics - ISEF2019*, Aug 2019, Nancy, France.

[10] K. Uppalapati and J. Bird, "A flux focusing ferrite magnetic gear," *6th IET International Conference on Power Electronics, Machines and Drives (PEMD 2012)*, March 2012, pp. 1–6.

[11] K. K. Uppalapati, J. Z. Bird, J. Wright, J. Pitchard, M. Calvin, and W.Williams, "A magnetic gearbox with an active region torque density of 239 Nm/L," *IEEE Energy Conversion Congress and Exposition (ECCE)*, 2014, pp. 1422-1428.

[12] I. Boldea and S. A. Nasar, The Induction Machines Design Handbook, 2nd edition, CRC Press, 2009.

[13] T. Lubin, S. Mezani, and A. Rezzoug, "Analytical computation of the magnetic field distribution in a magnetic gear," *IEEE Trans. Magn*., vol. 46, no. 7, pp. 2611–2621, Jul. 2010.

[14] M. G. Kesgin, P. Han, D. Lawhorn, D. M. Ionel, "Analysis of Torque Production in Axial-flux Vernier PM Machines of the MAGNUS Type," *IEEE Electric Machine and Drive Conference (IEMDC)*, June 2021.

BIOGRAPHIES

Badr-el-Boudour Bidouche received a master's degree in electrical energy in 2016 from the Graduate School Ense3 of Grenoble, France. She got her PhD in Electrical engineering in 2019 from the Lorraine University where she worked on the design of a magnetically geared induction machine at the "Groupe de Recherche en Energie Electrique de Nancy", GREEN of the Lorraine University, Nancy, France. Currently, she's a Technical Specialist, EM solutions at Altair Engineering developing applications and features for the FluxMotor software.

Thierry Lubin received the M.S. degree in electrical engineering from the University Pierre et Marie Curie, Paris, France, in 1994, and the Ph.D. degree from the University of Lorraine, Nancy, France, in 2003. He is an Associate Professor of electrical engineering with the Faculty of Sciences and Technology, University of Lorraine, Nancy, where his research works are undertaken in the Groupe de Recherche en Energie Electrique de Nancy (GREEN) Laboratory. His research interests include analytical modeling, design, and control of electrical machines, and the use of superconductors in electromechanical devices.

Smail Mezani received the Engineer diploma and master's degrees in electrical engineering from the University of Science and Technology Houari Boumediene, Bab Ezzouar, Algiers, in 1996 and 1999, respectively, and the Ph.D. degree from the Institut National Polytechnique de Lorraine, Nancy, France, in 2004.,He is an Associate Professor of electrical engineering with the Faculty of Sciences and Technology, University of Lorraine, Nancy, where his research works are undertaken in the Groupe de Recherche en Energie Electrique de Nancy (GREEN) Laboratory. His research interests include analytical and numerical modeling of conventional electrical machines and special electromechanical energy conversion devices, among which magnetic gears and magnetic couplers are made of conventional magnetic materials and superconductors.

Franck Vangraefschèpe received an engineering degree in Aeronautics from Supaero, Toulouse, France, in 1998 and a Master degree in Automotive from ENSPM, Rueil-Malmaison, France, in 2000. He first worked on combustion engines at IFPEN, Rueil-Malmaison, France, where he optimized efficiency and pollutant emissions of gasoline combustion. He then changed to work on Hybrid and Electric Vehicles globally, and on electric powertrains more specifically at VEDECOM. He is currently electric motors development project manager for aeronautic applications at IRT Saint-Exupery, Toulouse, France.

Tahar hamiti received the Ingenieur d'Etat degree in automatic control systems from the University of Tizi-Ouzou, Tizi Ouzou, Algeria, and the Ph.D. degree in electrical engineering from the University of Lorraine, Nancy, France. From 2010 to 2015, he was a Research Fellow and a Lecturer with the Power Electronics, Machines and Control Group, The University of Nottingham, Nottingham, U.K. In 2015, he joined VEDECOM, a French institute for energy transition to work on electrical machines for electric and hybrid vehicles. Since 2018, he has been with Nidec-PSA-Emotors, a Stellantis-Nidec joint venture dedicated to design, develop, and manufacture electrical powertrains for xEV. His research interests include modeling, design, and control of electrical machines for transportation applications and power generation.